Research Square

Preprints are preliminary reports that have not undergone peer review.
They should not be considered conclusive, used to inform clinical practice,
or referenced by the media as validated information.

Boosting visible-light-driven hydrogen evolution of polymer photocatalysts by a universal main-chain-engineering strategy of hydrophilic non-conjugated building blocks

Chih-Li Chang
National Tsing Hua University https://orcid.org/0000-0001-9497-7186
Wei-Cheng Lin
National Tsing Hua University
Li-Yu Ting
National Tsing Hua University
Chin-Hsuan Shih
National Cheng Kung University
Shin-Yuan Chen
National Institute of Advanced Industrial Science and Technology (AIST) https://orcid.org/0000-0002-7093-2511
Tse-Fu Huang
National Tsing Hua University
Hiroyuki Tateno
National Institute of Advanced Industrial Science and Technology (AIST) https://orcid.org/0000-0003-2395-2197
Jayachandran Jayakumar
National Tsing Hua University
Che-Yi Chu
National Chung Hsing University
Chin-Wen Chen
National Taipei University of Technology
Chi-Hua Yu
National Cheng Kung University https://orcid.org/0000-0001-9445-3358
Yu-Jung Lu
Academia Sinica https://orcid.org/0000-0002-3932-653X
Takehisa Mochizuki
National Institute of Advanced Industrial Science and Technology (AIST)
Ho-Hsiu Chou (hhchou@mx.nthu.edu.tw)
National Tsing Hua University https://orcid.org/0000-0003-3777-2277

Article

Keywords:

Posted Date: April 18th, 2022

DOI: https://doi.org/10.21203/rs.3.rs-1548164/v1

License: This work is licensed under a Creative Commons Attribution 4.0 International License.
Read Full License

Version of Record: A version of this preprint was published at Nature Communications on September 17th, 2022. See the published version at https://doi.org/10.1038/s41467-022-33211-1.

Abstract

Photocatalytic water splitting is attracting considerable interest because it enables abundant solar energy to be converted into hydrogen for use as a zero-emission fuel or chemical feedstock. Herein, we present a universal approach for inserting hydrophilic non-conjugated building blocks into the main-chain of conjugated polymers to produce a series of discontinuously conjugated polymer (DCP) photocatalysts. Water can effectively be brought into the interior of DCPs through these hydrophilic non-conjugated building blocks, resulting in effective water/polymer interfaces inside the bulk DCPs in both thin-film and solution. P-10HEG with 10 mol% ethylene glycol-based hydrophilic building blocks achieved a record high apparent quantum yield of 17.82% under 460 nm monochromatic light irradiation in solution and an excellent hydrogen evolution rate of 16.8 mmol m^{-2} h^{-1} in thin-film. Molecular dynamics simulation shows a trend similar to that in experiments, which confirms that main-chain engineering increases the possibility of a water-DCP interaction. Unlike the previous strategy of maintaining a long conjugation length, our approach results in DCP photocatalysts with an interrupted conjugation length that remains efficient photocatalysis.

Introduction

Inspired by natural photosynthesis, researchers are developing photocatalysts to efficiently convert abundant solar energy into low-carbon chemicals and fuels. Hydrogen is an attractive primary energy source for a carbon-neutral society because it produces only water and heat during combustion[1–3]. Therefore, photocatalytic water splitting to produce zero-emission hydrogen has attracted considerable attention in the effort to address global challenges related to energy crises and environmental pollution[4–6]. However, the development of efficient and stable photocatalysts that can suppress electron-hole recombination and facilitate electron transfer in the photocatalytic reaction remains a challenge because it requires well-managed light harvesting and effective engineering of the energy levels, photocatalytic interface, and reaction mechanism. Thus, it is imperative to develop a strategy for the systematic study of photocatalysts with precise control of their molecular structure.

In recent decades, most studies have focused on the fabrication of inorganic photocatalysts, particularly metal-based semiconductors, which have low photocatalytic activity in the visible region, require harsh fabrication conditions, and are difficult to optimize[7]. In 1985, Yanagida *et al.* first reported poly(*p*-phenylene) as an organic photocatalyst for hydrogen evolution during water splitting[8]. Since then, conjugated polymers (CPs) have attracted considerable attention[9–15]. Nevertheless, the main limitation of CPs with a hydrophobic skeleton is their nonhomogeneous dispersion under the conditions used for water-based reactions, where the use of an organic co-solvent is necessary. In addition, the severe aggregation of polymer chains and the poor water/polymer interfacial behavior limit electron transfer through the interface, and thus suppress hydrogen production via a two-electron process. Therefore, organic polymer photocatalysts with suitable hydrophilicity are potential candidates for water splitting with less/no organic co-solvent. Recently, many groups and us demonstrated that the hydrogen evolution

rate (HER) of hydrophobic CP photocatalysts could be significantly increased under water-based photocatalytic conditions when covered with amphipathic small molecules or polymer surfactants[16–22].

In another strategy, hydrophilic functional groups (e.g., ethylene glycol, carboxylic acid, amino and ionic electrolyte groups) are incorporated on the side-chain of hydrophobic CPs to intrinsically improve the hydrophilicity of the CPs[23–26]. Although all previous studies introduced such hydrophilic groups on the side-chains of CPs, the backbones of side-chain-engineered CPs are hydrophobic, similar to those of conventional CPs. These previous studies considered that a long conjugation length was necessary for polymer photocatalysts to achieve better charge transport; however, the ideal conjugation length for photocatalytic hydrogen evolution is still unclear. The interior of the bulk side-chain-engineered CPs was still affected by the same issue as conventional CPs, resulting in intense electron-hole recombination and a poor water/polymer interface. Moreover, side-chain engineering is restricted to specific structures and results in poor applicability. Herein, for the first time, main-chain-engineered DCPs were achieved through a delicate balance of hydrophilic non-conjugated building blocks and hydrophobic conjugated building blocks, resulting in an enhanced water/polymer interface to facilitate photocatalytic hydrogen evolution (Fig. 1a). Importantly, the types and contents of hydrophilic non-conjugated building blocks can be easily tuned and polymerized with various conjugated building blocks, which shows higher possibility and flexibility in our main-chain-engineered strategy.

Results

Polymer synthesis and characterization. To demonstrate our design strategy, poly[(9,9-dioctyl-9*H*-fluorenyl-2,7-diyl)-*co*-(5-phenylbenzo[*b*]phosphindole-5-oxide-2,7-diyl)] (PFBPO) with a hydrophobic backbone was chosen as the reference CP for comparison with the DCPs because of its relatively high HER in visible-light-driven photocatalytic reactions[27]. We designed ethylene glycol (EG)- and ethylene diamine (EA)-based hydrophilic non-conjugated building blocks and incorporated them into the backbone of PFBPO. We synthesized EG- and EA-based DCPs via Pd-catalysed Suzuki–Miyaura coupling polymerization of fluorene-boronic ester and 3,7-dibromo-5-phenylbenzo[b]phosphindole-5-oxide with either EG-based (EG-Br, TEG-Br, and HEG-Br) or EA-based (EA-Br) building blocks. The hydrophilic non-conjugated building blocks were covalently bonded to the backbone of PFBPO at various ratios (5, 10, and 20 mol%), resulting in seven DCP photocatalysts, denoted P-5EG, P-5TEG, P-5HEG, P-10HEG, P-20HEG, P-5EA and P-10EA (Fig. 1b, Supplementary scheme 1). First, the monomers were synthesized and their chemical structures were identified by NMR spectroscopy and mass spectrometry (Supplementary Fig. 1–8). The monomers were then polymerized into the corresponding EG- and EA-based DCPs, the chemical structures of which were investigated in detail using NMR and FT-IR spectroscopy. The ^{1}H NMR spectra (Supplementary Figs. 9–15) showed characteristic signals of the EG- and EA-based building blocks at 3.5–4.5 ppm, indicating that hydrophilic non-conjugated groups were present in the polymer backbones. The intensities of the characteristic signals of HEG-Br and EA-Br in the DCP backbones clearly increased with increasing molar fractions of the HEG-Br and EA-Br monomers during polymerization (Supplementary Figs. 11–15). Characteristic NMR and FT-IR signals of the phosphine oxide groups were

observed at 33.80 ppm (Supplementary Fig. 16–22) and 1140–1210 cm^{-1} (Supplementary Fig. 23), respectively. The molecular weight and polydispersity index of the DCPs were determined using gel permeation chromatography (Supplementary Table 1). The results of thermogravimetric and X-ray diffraction analyzes indicated that all prepared polymers had an amorphous framework that was highly stable in a nitrogen atmosphere (T_d > 400 °C; see Supplementary Figs. 24–25).

Optical properties. The optical properties, optical band gap (E_g), and energies of the highest occupied molecular orbital (HOMO) and lowest unoccupied molecular orbital (LUMO) of the DCPs were studied by diffuse reflectance UV–vis spectroscopy (DRS), photoluminescence spectroscopy, and photoelectronic spectroscopy. The DRS of the DCPs was very similar to that of PFBPO (Fig. 2a). The HOMO levels of the DCPs ranged from −5.90 to −5.93 eV, as measured using a photoelectronic spectrometer (Supplementary Fig. 26). The LUMO levels were calculated using $E_{LUMO} = E_{HOMO} + E_g$, where the E_g values of the DCPs calculated from Tauc plots were close to 2.75 eV (Fig. 2b); the LUMO levels ranged from −3.15 to −3.20 eV, indicating that hydrogen evolution was thermodynamically favourable (Table 1). The differences between the HOMO/LUMO levels and the optical E_g were small, indicating that hydrophilic non-conjugated building blocks could be molecularly engineered into the main-chain of the target CPs using the present approach without significantly affecting the physicochemical and optical properties (Fig. 2c). The photoluminescence spectra show that both DCPs and PFBPO were effectively quenched by adding Pt co-catalysts (Fig. 3a). The photoluminescence quenching of P-5EG, P-10HEG, and P-5EA was higher than that of PFBPO, indicating that the charge transfer from DCPs to the Pt co-catalysts was improved. The time-resolved photoluminescence spectra (Fig. 3b) show that the lifetimes of the excited states of the DCPs were 1.02–1.22 ns. The P-10HEG had the longest lifetime, and all of the DCPs had longer lifetimes than PFBPO (0.84 ns), suggesting that the recombination rates of the electron–hole pairs were effectively reduced.

Table 1. Photophysical properties and HERs of various polymers.

Polymer	$\lambda_{max,\ abs}$ (nm)[a]	Size (nm)[b]	HOMO (eV)[c]	LUMO (eV)[d]	E_g (eV)[e]	Lifetime (ns)[f]	HER $780 > \lambda > 380$ nm (μmol h^{-1})[g]	HER $780 > \lambda > 380$ nm (mmol h^{-1} g^{-1})[g]
PFBPO	410	471	-5.82	-3.13	2.69	0.84	23.0 ± 1.85	4.60 ± 0.37
P-5EG	410	654	-5.92	-3.18	2.74	1.03	23.9 ± 2.60	4.78 ± 0.52
P-5TEG	408	674	-5.91	-3.19	2.72	1.02	25.8 ± 1.35	5.16 ± 0.27
P-5HEG	414	686	-5.91	-3.16	2.75	1.11	26.9 ± 1.55	5.38 ± 0.31
P-10HEG	402	1129	-5.92	-3.16	2.76	1.22	34.7 ± 3.45	6.94 ± 0.69
P-20HEG	390	1576	-5.90	-3.20	2.70	1.11	18.7 ± 1.80	3.74 ± 0.36
P-5EA	402	957	-5.93	-3.20	2.73	1.12	30.3 ± 3.05	6.06 ± 0.61
P-10EA	396	1434	-5.91	-3.15	2.76	1.07	19.4 ± 1.95	3.88 ± 0.39

[a]Determined by solid-state UV-vis diffuse reflectance spectroscopy; [b]Determined by DLS; [c]Determined by photoelectron spectroscopy; [d]Determined by means of the equation E_{LUMO}

= E_{HOMO} + E_g; [e]Determined from Tauc plots; [f]Determined by time-resolved fluorescence spectroscopy; [g]Photocatalytic conditions: 5 mg of polymers dissolved in a 10 mL mixture solution (H_2O/MeOH/TEA) and irradiated by a simulated solar light source (300 W Xe lamp, 1000 W m^{-2}, 780 > λ > 380 nm).

Electrochemical properties. Electron paramagnetic resonance (EPR), electrochemical impedance spectroscopy (EIS), and transient photocurrent measurements were used to characterize the charge generation, transport, and transfer upon irradiation of the DCPs. In the EPR spectra (Fig. 3c, Supplementary Fig. 27), a sharp signal was observed at 3500–3520 G and its intensity increased with light irradiation due to radical generation via photoexcitation. The irradiation-induced signal enhancement for the DCPs was greater than that for PFBPO. The EIS data recorded in the dark showed a semicircular curve (Fig. 3d), where the DCPs had resistance values lower than that of PFBPO due to their enhanced charge transport. Transient photocurrent measurements (Fig. 3e) used to investigate the photoresponse of the DCPs showed that these materials responded quickly to light irradiation and their photocurrents were higher than that of PFBPO. Hence, hydrophilic building blocks may exhibit a suitable interface with water to facilitate charge transport and transfer. Cyclic voltammetry analysis of P-10HEG showed that this material was highly electrochemically stable with a reversible reduction–oxidation cycle in the range from −0.2 V to −1.1 V for at least 15 cycles (Fig. 3f).

Morphology and hydrophilicity. Scanning electron microscopy (SEM; Supplementary Fig. 28–35) images showed that the solid DCPs consisted of small particles with similar morphologies and microscale sizes, independent of the hydrophilic non-conjugated building blocks. The water contact angles of the EG-Br, TEG-Br, HEG-Br, and EA-Br monomers were 95.7°, 82.1°, 47.4°, and 76.7°, respectively (Supplementary Fig. 36), where HEG-Br had the highest hydrophilicity (lowest contact angle). Interestingly, we measured the contact angles of water drop on all of the DCPs films promptly, and observed hydrophobic behaviour with the contact angles of approximately 109° (Supplementary Fig. 37), which were in contrast to most side-chain-engineered CPs that show hydrophilic behavior[19-22]. This result implies that the type and content of hydrophilic non-conjugated building blocks in the hydrophobic CPs do not significantly affect the hydrophilicity of the DCP films due to packing of the polymers. The particle size distributions of the DCPs in a H_2O/methanol (MeOH)/triethylamine (TEA) (1:1:1 by volume) solution were determined by dynamic light scattering (DLS). The DLS results (Supplementary Fig. 38) indicated a wide range of hydrodynamic diameters for PFBPO P-5EG, P-5TEG, P-5HEG, P-10HEG, P-20HEG, P-5EA, and P-10EA of 471, 654, 674, 686, 1129, 1576, 957, and 1434 nm, respectively. All of these values were larger than that of PFBPO, indicating that the DCPs swelled in the aqueous solution[28,29]. Hence, the hydrophilicity of the DCPs could be tuned by using different types or contents of hydrophilic non-conjugated building blocks to allow water to penetrate the bulk of the polymer in the solution state. To further investigate the morphology of the DCPs, small-angle X-ray scattering (SAXS) measurements were performed by dispersing the DCPs in a 1:1:1 H_2O/MeOH/TEA solution and comparing their architectures. The intermediate- and high-q scattering characteristics (q = 0.4–4 nm^{-1}) shown in the SAXS patterns of P-5HEG, P-10HEG, and P-

20HEG (Supplementary Fig. 39) were ascribed to a one-dimensional rod geometry with polydispersity in the rod size[30]. Fitting of the high-q scattering profile indicated that the DCPs formed rod-like bundles in aqueous solution and that their length (2 ± 0.004 nm) was independent of the content of hydrophilic non-conjugated building blocks. However, the low-q scattering profile ($q < 0.4$ nm^{-1}) of P-10HEG was fitted with the lowest power law exponent of -2.0, revealing that the rod-shaped bundles of P-10HEG can be further organized into an aggregated structure with a random distribution. The lower degree of aggregation implied a loose arrangement of the polymer bundles, resulting in a larger interfacial area.

Photocatalytic hydrogen evolution. The photocatalytic hydrogen evolution of the DCPs was measured at 25 °C under visible-light irradiation (λ = 380–780 nm) and compared to that of PFBPO. Fig. 4a shows that the HER values of the DCPs with 5–10 mol% hydrophilic non-conjugated building blocks were clearly higher than that of PFBPO. In particular, a stable HER of P-10HEG was observed with increasing reaction time, and an excellent HER of 34.7 μmol h^{-1} was obtained, which was approximately 50% higher than that of PFBPO (23.0 μmol h^{-1}). The hydrophilic non-conjugated building blocks facilitated the swelling of the polymer aggregates in the presence of water and thus enhanced the HER of the DCPs (Table 1). However, the HER of P-20HEG (with 80 mol% BPO active building blocks and 20 mol% HEG hydrophilic building blocks) was lower, with a value of 18.7 μmol h^{-1}. Therefore, the optimal content of hydrophilic HEG building blocks on the backbone of DCPs was approximately 10 mol%. Considering the SAXS results, the fact that P-10HEG exhibited the highest HER was closely related to its loose aggregates, which provide a high interfacial area for hydrogen evolution.

The P-5EA sample also showed a high HER of 30.3 μmol h^{-1}, which was higher than those of its counterparts with 5 mol% EG-based hydrophilic building blocks (e.g., P-5EG, P-5TEG, and P-5HEG). The EA-based hydrophilic building blocks with N-containing functional groups experienced stronger hydrogen bonding with water than the EG-based hydrophilic building blocks with oxygen-containing functional groups. In addition, when 10 mol% EA was present, the corresponding P-10EA exhibited a relatively low HER of 19.4 μmol h^{-1}. In the EA-based DCPs, the optimal content of EA hydrophilic building blocks on the backbones of the DCPs was approximately 5 mol%. As seen from the DLS data, P-10HEG and P-5EA were significantly swollen with water in the H_2O/MeOH/TEA solution, forming aggregates with a diameter of approximately 1000 nm, which were suitable for water-based photocatalytic hydrogen evolution. It was demonstrated that the HER of polymer photocatalysts can indeed be increased by diffusing more water into the active building blocks via main-chain engineering of hydrophilic building blocks within the backbones of hydrophobic CPs.

Similar results were found when the concentrations of CPs and DCPs in the photocatalytic solution were increased. The HER of PFBPO was 23.0 μmol h^{-1} in a 5 mg/10 mL solution, and it increased only 1.3–1.6 times in 10–15 mg/10 mL solutions (Fig. 4b, Supplementary Table 1). However, the HER of P-10HEG increased 1.5, 2.9, and 3.5 times in 5 mg/10 mL (HER = 34.7 μmol h^{-1}), 10 mg/10 mL (HER = 66.1 μmol h^{-}

^{1}), and 15 mg/10 mL (HER = 81.6 μmol h^{-1}) solutions, respectively, compared to that of PFBPO in the 5 mg/10 mL photocatalytic solution. Notably, P-20HEG exhibited a higher HER than PFBPO in 10 mg/10 mL and 15 mg/10 mL solutions, demonstrating that the optimized concentration saturation of the DCPs was much higher than that of the respective CPs. This finding suggests that increasing the concentration of CPs in a photocatalytic solution enhances their aggregation, so that the inner polymer chains of the CPs cannot interact effectively with the water. Likewise, a linear increase in the HER was observed with increasing quantity of photocatalytic solutions in the absence of a Pt co-catalyst (Fig. 4c, Supplementary Fig. 40), demonstrating that, at a fixed concentration, the total amount of hydrogen production could be increased by increasing the reactor size. Apparent quantum yield (AQY) values were obtained under standard photocatalytic conditions using a light source with a bandpass filter (λ = 420, 460, 500, 550, or 600 nm). Without a Pt co-catalyst, P-10HEG exhibited high AQYs of 18.19% and 17.82% at 420 and 460 nm, respectively (Fig. 4d, Supplementary Table 2). The trend in AQY values as a function of wavelength was very similar to that of the UV-vis absorption spectra of P-10HEG, indicating that photocatalytic hydrogen evolution occurred via light harvesting. Taking advantage of the strong interaction between the hydrophilic non-conjugated building blocks and the Pd co-catalyst, which can enhance the charge separation and transfer at the interfacial area[26,31], the HER of P-10HEG with 5 wt.% Pt co-catalyst was increased to 54.1 μmol h^{-1} (10.82 mmol h^{-1} g^{-1}) (Supplementary Fig. 41).

We further verified the performance of the DCPs for photocatalytic hydrogen evolution in the absence of MeOH (i.e., in a H_2O/TEA solution, Fig. 4e). PFBPO exhibited a very low HER (6.79 μmol h^{-1}), while P-10HEG and P-5EA exhibited values of up to 22.8 μmol h^{-1} and 18.6 μmol h^{-1}, respectively, in the H_2O/TEA solution, and these values were close to that of PFBPO in the presence of MeOH (23.0 μmol h^{-1}). Therefore, the introduction of 5–10 mol% HEG-Br or EA-Br hydrophilic building blocks on the main-chain of DCPs could replace the use of the typically used 33 vol.% MeOH. In addition, compared to side-chain engineering of CPs (containing 50 mol% hydrophilic building blocks), our approach required a smaller amount of hydrophilic building blocks (5–10 mol%) and could effectively increase the interaction between water and the inner active sites of the CPs to increase the HER. To further demonstrate the advantages and applicability of our design approach, we synthesized a side-chain-engineered CP (denoted as PFTEGBPO) to compare its photocatalytic HER with that of the P-10HEG DCPs (Fig. 4f, Supplementary Fig. 42). The results proved that our main-chain engineering strategy utilized the inner active sites of CPs more effectively than the side-chain engineering strategy. Furthermore, to demonstrate the universality of our approach, we extended the hydrophilic HEG-Br building block to polymerize with other donor–acceptor CPs. A PF8BT-10HEG sample was synthesized by the main-chain engineering of 10 mol% HEG-Br into the backbone of a PF8BT, which exhibited an enhanced HER compared to that of PF8BT (Supplementary Fig. 43), proving that this approach can be easily applied to different CPs.

Furthermore, we coated the PFBPO and P-10HEG to obtain uniform films on silicon wafers by only single dropcast cycle (Fig. 5a,b). As shown in Fig. 5c and Supplementary Table 3, the P-10HEG showed a record high HER of 16.6 mmol m^{-2} h^{-1} in a film state. Interestingly, the HER of P-10HEG showed 2-times enhancement compared to that of PFBPO, which is higher than the enhancement in solution state (1.5-

times). We also measured the water contact angle of film photocatalysts over a period of time to determine the wetting effect of these films (Fig. 5d,e). In the case of the P-10HEG film with the initial contact angle of 107.9° and then decreased to 65.5° over the period of 20 minutes. While for the PFBPO film, the initial water contact angle of 112.0° decreased to 79.3° after 20 minutes. Since the molecular packing of polymer in film state is severe than that in solution state, resulting the inside of the polymer film may not react with water efficiently, this result demonstrated the advantage of our main-chain engineered DCP as film photocatalysts.

Molecular dynamics simulation provides a microscale understanding of the interaction between water and DCP. Improvement in hydrogen results from a higher possibility of hydrogen bond formation. To further examine the mechanisms at the microscale, we considered three different models: a non-conjugate block located at the middle, one-third, and the end of the polymer chain. Here, we consider that the DCPs are composed mainly of these three configurations with different weight percentages. Fig. 6a shows the average number of hydrogen bond formations for different DCPs. The statistic of hydrogen bounds suggest that the system composed of 80% of the DCP with conjugate monomer located at the center, 15% at 1/3 of the overall chain, and 5% at the end, in agreement with the trend of experimental findings. Fig. 6b plots the radial distribution function and the morphology of each DCP chain. One can observe that DCP with 10 mol% HEG-modified exhibits the highest possibility of hydrogen bond formation and the probability of radial distribution function. In contrast, a 10 mol% EA-modified DCP shows a relatively low possibility of hydrogen bond formation. Simulation results also reveal that 10 mol% HEG-modified and 5 mol% EA-modified DCPs were entangled more than other DCP systems where other DCPs remained in single-chain formation.

Discussion

For the first time, we successfully developed a series of DCPs by inserting hydrophilic non-conjugated building blocks into the main-chain of hydrophobic CPs to produce photocatalysts with high HERs under visible-light irradiation. The DCPs with interrupted conjugation showed enhanced HER values in both the film state and the solution state compared to those of their hydrophobic photocatalyst counterparts under otherwise identical conditions. The hydrophilic non-conjugated building blocks effectively brought water into the inner polymer chain of main-chain-engineered DCPs, which increased the HER without obviously changing the semiconducting properties of the polymers, thereby overcoming a major limitation in the field. DCPs with hydrophilic building blocks of 5–10 mol% exhibited HERs comparable to those of hydrophobic CPs with the use of 33 vol.% organic solvent. Furthermore, in this study, we exploited a full atomistic study using molecular dynamics simulation to elucidate the interaction between water and DCPs which agrees well with the experimental measurements. This indicates that main-chain engineering using hydrophilic non-conjugated building blocks increases the possibility of water-DCP interaction and is more efficient in comparison with ordinary conjugate polymers. Importantly, we also demonstrated that our proposed approach is a universal route for synthesizing new classes of DCPs with enhanced photocatalytic hydrogen evolution. The use of hydrophilic non-conjugated building blocks in the main-chain engineering of semiconducting polymers could lead to further optimization and greater

molecular-design possibilities for developing high-performance photocatalysts for the generation of clean and renewable energy and future industrial applications.

Methods

Synthesis of polymer photocatalysts. Toluene and water were injected into a sealed tube charged with the co-monomers, K_2CO_3, tetra-*n*-butylammonium bromide (TBAB), and $Pd(PPh_3)_4$. The mixture was degassed by bubbling with nitrogen for 30 min and then heated at 120°C for 48 h. After cooling to 25°C, bromobenzene was added and then the sealed tube was heated at 120°C for 6 h, followed by addition of phenyl boronic acid and heating at 120°C for another 6 h. The mixture was cooled to 25°C and poured in MeOH. The precipitate was collected using membrane filtration. Purification of the polymer was performed through Soxhlet extraction with MeOH and hexane. Finally, the polymer was dissolved in hot $CHCl_3$, concentrated, and then precipitated in MeOH. The polymer was collected and dried under vacuum.

Photocatalytic hydrogen evolution. Hydrogen was detected using a Shimadzu GC-2014 gas chromatograph equipped with a thermal conductivity detector, with Ar as carrier gas. In a typical measurement, the reaction cuvette was charged with 5 mg of polymer powder and 10 mL of the mixture solution (H_2O, MeOH, TEA (1:1:1 by volume)) and sealed with a septum. The resulting mixture was degassed by bubbling with argon gas for 10 min, prior to illumination. The suspension was illuminated with a 350-W Xe-lamp (1000 W/m^2, $\lambda > 420$ nm), maintaining its temperature at 27 ± 1 °C under atmospheric pressure and keeping the distance between the reaction mixture and light source fixed.

Photocurrent measurements. A Zahner Zennium E works station equipped with three-electrode cell consists of Ag/AgCl as reference electrode (3 M NaCl), Pt wire as counter electrode, and fluorine doped tin oxide (FTO) glass as working electrode. The polymer sample (5 mg) was dispersed in dry toluene solution (1 mL) and ultra-sonicated for 1 h. Then, 200 µL of the as-prepared polymer suspension was spin-coated on FTO-glass with an active area of 1.0 cm^2. The electrolyte was an aqueous solution of 0.5 M Na_2SO_4. We measured the photocurrent generated using LED irradiation (constant potential = 1.5 V) with the light switched on-off with intervals of 20 s.

Molecular dynamics. Molecular simulations were performed by Materials Studio. An overall workflow is depicted in Fig. 6a. We adopted the Dreiding force field as the interatomic potential, and built a single chain model in the center of the periodic box. Before dynamic simulations, geometry optimization was performed to relax the artificial polymer chain to obtain a suitable initial model. Then, the NVT ensemble was chosen to run the dynamic simulations at a temperature of 298 K in 1 ns for relaxing the polymer chain within the water. Finally, the NPT ensemble was adopted to drive with a temperature and pressure of 298K and 1 atm, respectively, for 1 ns to obtain an equilibrium structure. After dynamic simulations, the trajectory file was analyzed to obtain the radial distribution function to predict the possibility of hydrogen bond formation in Fig. 6b, and the number of hydrogen bonds over unit volume was also statistical, as shown in Fig. 6a.

References

1. Tachibana, Y., Vayssieres, L. & Durrant, J. R. Artificial photosynthesis for solar water-splitting. Nat. Photonics **6**(8), 511–518 (2012). 10.1038/nphoton.2012.175
2. Barber, J. Photosynthetic energy conversion: natural and artificial. Chem. Soc. Rev. **38**(1), 185–196 (2009). 10.1039/b802262n, https://www.ncbi.nlm.nih.gov/pubmed/19088973
3. Jayakumar, J. & Chou, H.-H. Recent advances in visible-light-driven hydrogen evolution from water using polymer photocatalysts. ChemCatChem **12**(3), 689–704 (2020). 10.1002/cctc.201901725
4. Zhang, G., Lan, Z. A. & Wang, X. Surface engineering of graphitic carbon nitride polymers with cocatalysts for photocatalytic overall water splitting. Chem. Sci. **8**(8), 5261–5274 (2017). 10.1039/c7sc01747b, https://www.ncbi.nlm.nih.gov/pubmed/28959425
5. Wang, Y. *et al*. Current understanding and challenges of solar-driven hydrogen generation using polymeric photocatalysts. Nat. Energy 4(1), 746–760 (2019).
6. Kudo, A. & Miseki, Y. Heterogeneous photocatalyst materials for water splitting. Chem. Soc. Rev. **38**(1), 253–278 (2009). 10.1039/b800489g, https://www.ncbi.nlm.nih.gov/pubmed/19088977
7. Chen, X., Shen, S., Guo, L. & Mao, S. S. Semiconductor-based photocatalytic hydrogen generation. Chem. Rev. **110**(11), 6503–6570 (2010). 10.1021/cr1001645, https://www.ncbi.nlm.nih.gov/pubmed/21062099
8. Yanagida, S., Kabumoto, A., Mizumoto, K., Pac, C. & Yoshino, K. Poly(p-phenylene)-catalysed photoreduction of water to hydrogen. Chem. Commun. **8**, 474–475 (1985). 10.1039/C39850000474
9. Wang, X. *et al.* A metal-free polymeric photocatalyst for hydrogen production from water under visible light. Nat. Mater. **8**, 76–80 (2009). 10.1038/nmat2317
10. Sprick, R. S. *et al.* Tunable Organic Photocatalysts for Visible-Light-Driven Hydrogen Evolution. J. Am. Chem. Soc. **137**(9), 3265–3270 (2015). 10.1021/ja511552k
11. Vyas, V. S. *et al.* A tunable azine covalent organic framework platform for visible light-induced hydrogen generation. Nat. Commun., **6**(1), 8508 (2015). 10.1038/ncomms9508
12. Li, L. *et al.* Rational Design of Porous Conjugated Polymers and Roles of Residual Palladium for Photocatalytic Hydrogen Production. J. Am. Chem. Soc. **138**(24), 7681–7686 (2016). 10.1021/jacs.6b03472
13. Sachs, M. *et al.* Understanding structure-activity relationships in linear polymer photocatalysts for hydrogen evolution. Nat. Commun. **9**(1), 4968 (2018). 10.1038/s41467-018-07420-6, https://www.ncbi.nlm.nih.gov/pubmed/30470759
14. Wang, X. *et al.* Sulfone-containing covalent organic frameworks for photocatalytic hydrogen evolution from water. Nat. Chem. **10**(12), 1180–1189 (2018). 10.1038/s41557-018-0141-5, https://www.ncbi.nlm.nih.gov/pubmed/30275507
15. Ting, L.-Y. *et al.* Effect of controlling the number of fused rings on polymer photocatalysts for visible-light-driven hydrogen evolution. J. Mater. Chem. A **7**(40), 22924–22929 (2019). 10.1039/C9TA06425G

16. Zhao, P. *et al.* Hyperbranched conjugated polymer dots: the enhanced photocatalytic activity for visible light-driven hydrogen production. Macromolecules **52**(11), 4376–4384 (2019). 10.1021/acs.macromol.9b00551
17. Aitchison, C. M., Sprick, R. S. & Cooper, A. I. Emulsion polymerization derived organic photocatalysts for improved light-driven hydrogen evolution. J. Mater. Chem. A **7**(6), 2490–2496 (2019). 10.1039/C8TA11383A
18. Kosco, J. *et al.* Enhanced photocatalytic hydrogen evolution from organic semiconductor heterojunction nanoparticles. Nat. Mater. **19**(1), 559–565 (2020). 10.1038/s41563-019-0591-1
19. Pati, P. B. *et al.*. An experimental and theoretical study of an efficient polymer nano-photocatalyst for hydrogen evolution. Energy Environ. Sci. **10**(6), 1372–1376 (2017). 10.1039/C7EE00751E
20. Tseng, P.-J. *et al*. Design and synthesis of cycloplatinated polymer dots as photocatalysts for visible-light-driven hydrogen evolution. ACS Catal. **8**(9), 7766–7772 (2018). 10.1021/acscatal.8b01678
21. Chang, C.-L. *et al.* Sequence and secondary structure of Drosophila melanogaster 5.8S and 2S rRNAs and of the processing site between them. Appl. Catal. B **268** (2019). http://www.ncbi.nlm.nih.gov/pubmed/118436
22. Lin, W.-C. *et al.* Design and synthesis of cyclometalated iridium-based polymer dots as photocatalysts for visible light-driven hydrogen evolution. Int. J. Hydr. Energy **45**(56), 32072–32081 (2020). 10.1016/j.ijhydene.2020.08.288
23. Diao, R. *et al.* Significant improvement of photocatalytic hydrogen evolution of diketopyrrolopyrrole-based donor–acceptor conjugated polymers through side-chain engineering. Polym. Chem. **10**(47), 6473–6480 (2019). 10.1039/C9PY01404G
24. Chen, B., Yang, N., Wang, P., Xiang, Y. & Chen, H. Post-side chain engineering of difluorinated benzothiadiazole-based conjugated microporous polymer for enhanced photocatalytic H_2 evolution. Appl. Surf. Sci. **499**, 143865 (2020). 10.1016/j.apsusc.2019.143865.
25. Lin, K. *et al.* Amino-functionalised conjugated porous polymers for improved photocatalytic hydrogen evolution. J. Mater. Chem. A **7**, 19087–19093 (2019). 10.1039/C9TA06219J.
26. Hu, Z. *et al.* Conjugated Polymers with Oligoethylene Glycol Side Chains for Improved Photocatalytic Hydrogen Evolution. *iScience* **13**, 33–42 (2019). 10.1016/j.isci.2019.02.007, https://www.ncbi.nlm.nih.gov/pubmed/30818223
27. Wang, W.-H. *et al.* Design and synthesis of phenylphosphine oxide-based polymer photocatalysts for highly efficient visible-light-driven hydrogen evolution. Sustain. Energy Fuels **4**(10), 5264–5270 (2020). 10.1039/D0SE00928H
28. Ugelstad, J., Mork, P. C., Herder Kaggerud, K., Ellingsen, T. & Berge, A. Swelling of oligomer-polymer particles. New methods of preparation. Adv. Colloid Interface Sci. **12**, 101–140 (1980)
29. Sweijen, T., van Duijn, C. J. & Hassanizadeh, S. M. A model for diffusion of water into a swelling particle with a free boundary: Application to a super absorbent polymer particle. Chem. Eng. Sci. **172**, 407–413 (2017). 10.1016/j.ces.2017.06.045

30. Roe, R.-J. *Methods of X-ray and Neutron Scattering in Polymer Science*; Oxford University Press: New York, 2000
31. Lau, V. W.-H. *et al.* Rational design of carbon nitride photocatalysts by identification of cyanamide defects as catalytically relevant sites. Nat. Commun. **7**(1), 12165 (2016). 10.1038/ncomms12165

Declarations

Acknowledgements

The authors gratefully acknowledge the financial support of the Ministry of Science and Technology of Taiwan (MOST 111-2628-E-007-009-; MOST 110-2622-8-007-011-). The authors appreciate the assistance of the Precision Instrument Support Center of National Tsing Hua University in providing the analysis and measurement facilities. The computing resources were supported by TAIWANIA at the National Center for High-Performance Computing (NCHC) in Taiwan.

Author contributions

C.-L. C. designed, planned, and performed the experiments and wrote the manuscript. W.-C. L., L.-Y. T., and T.-F. H. prepared the polymer photocatalysts. J. J. carried out the transient experiments. C.-H. S., C.-W. C., and C.-H. Y. performed the MD calculations. S.-Y. C., H. T., T. M., and Y.-J. L. assisted in the experiments and characterizations. C.-Y. C. performed the SAXS experiments. H.-H. C. supervised the work on polymer synthesis and photocatalysis. All the authors participated in the interpretation and discussion of the results.

Competing interests

The authors declare no competing interests.

Figures

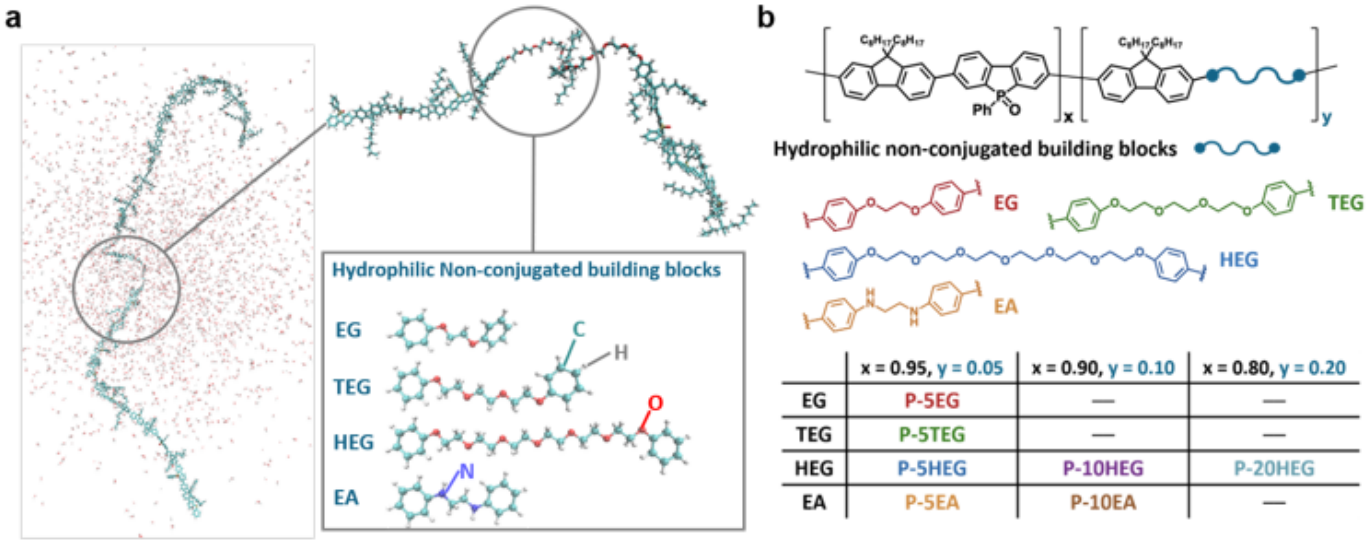

Figure 1

Schematic illustration and polymer structures. a Schematic illustration of the polymer photocatalysts containing hydrophilic non-conjugated building blocks. **b** The chemical structures of hydrophilic monomers and the corresponding DCPs.

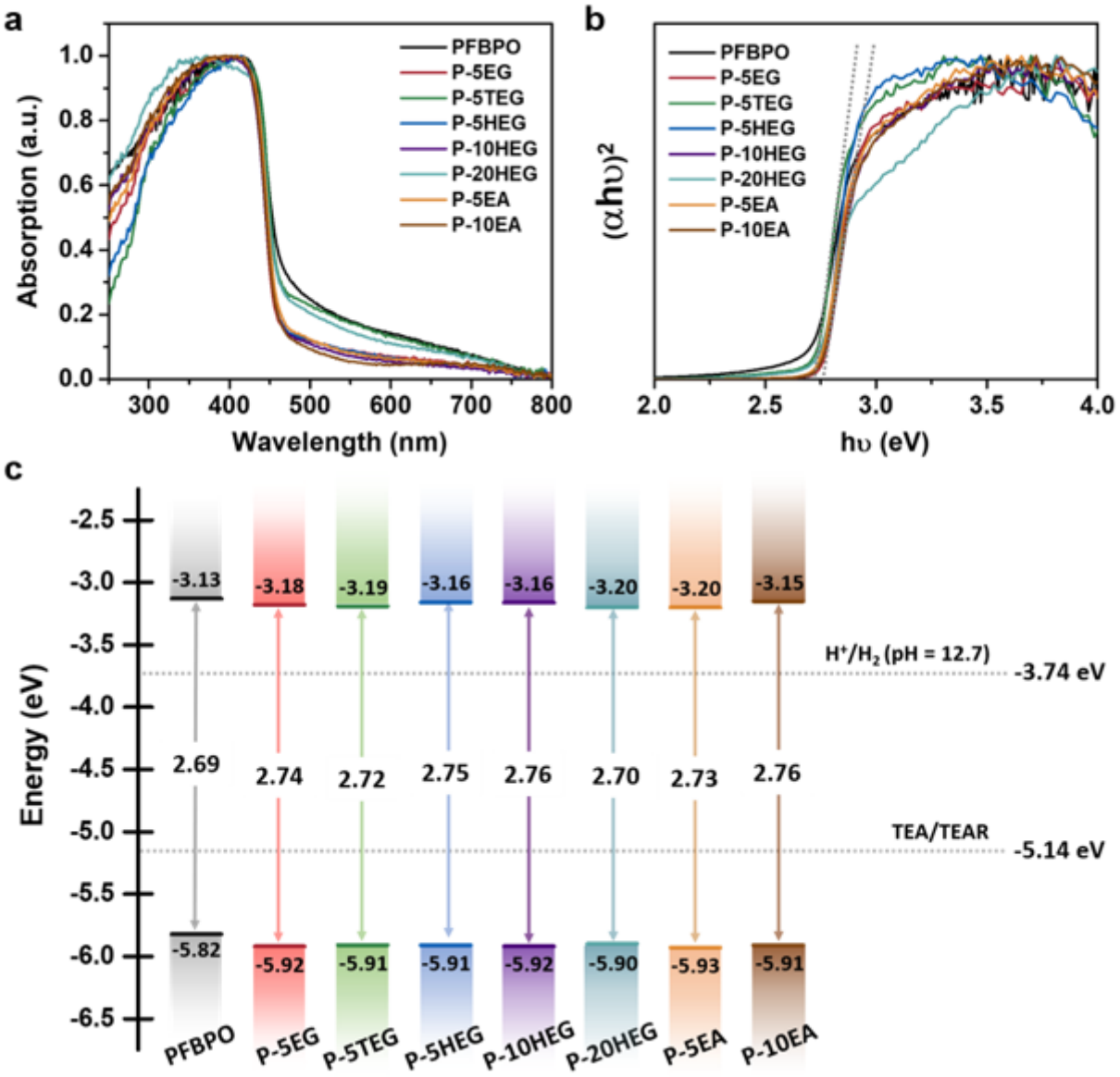

Figure 2

Optical properties of polymers. a Solid-state UV-vis diffuse reflectance spectra, **b** Tauc plots, and **c** energy-level diagram of polymer photocatalysts.

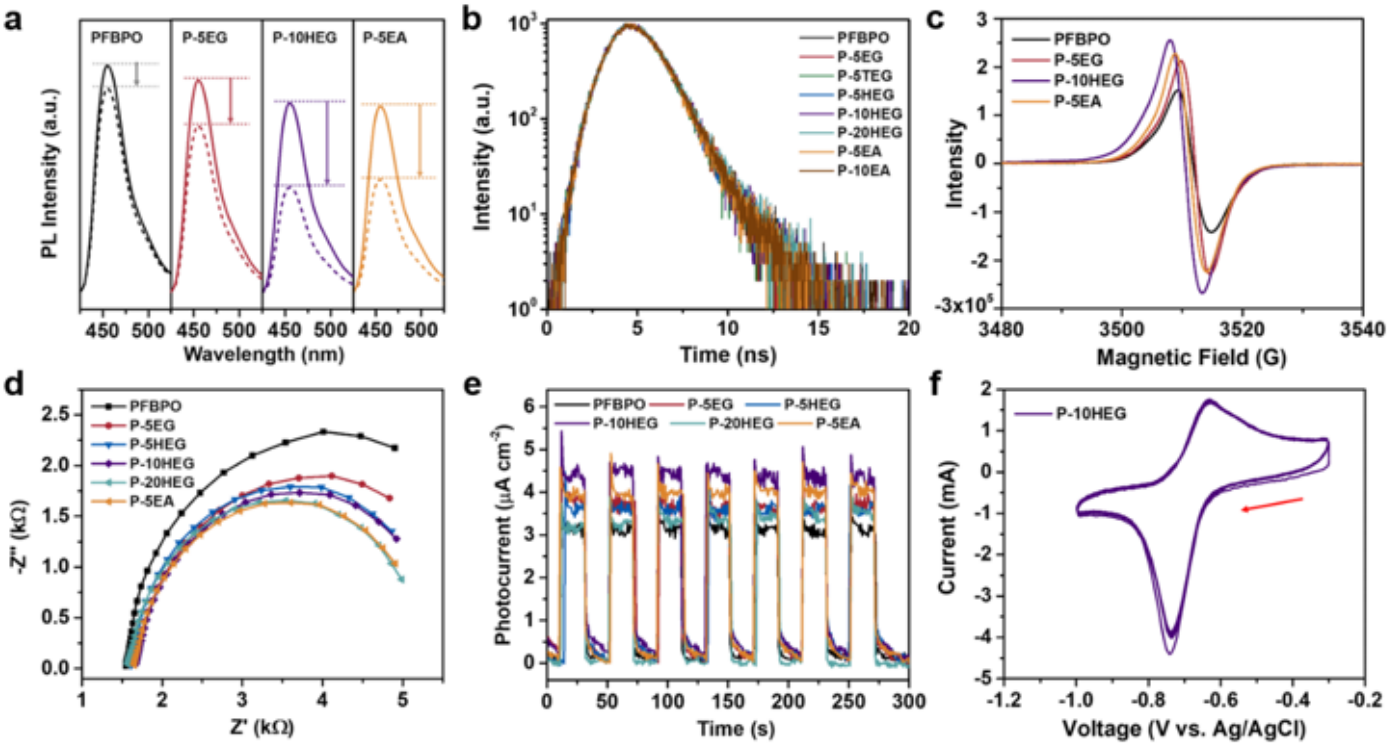

Figure 3

Electrochemical properties of polymers. a Photoluminescence emission spectra, **b** time-resolved photoluminescence spectra, **c** EPR spectra, **d** photocurrent, and **e** Nyquist plots of polymer photocatalysts and **f** cyclic CV reduction curves of P-10HEG.

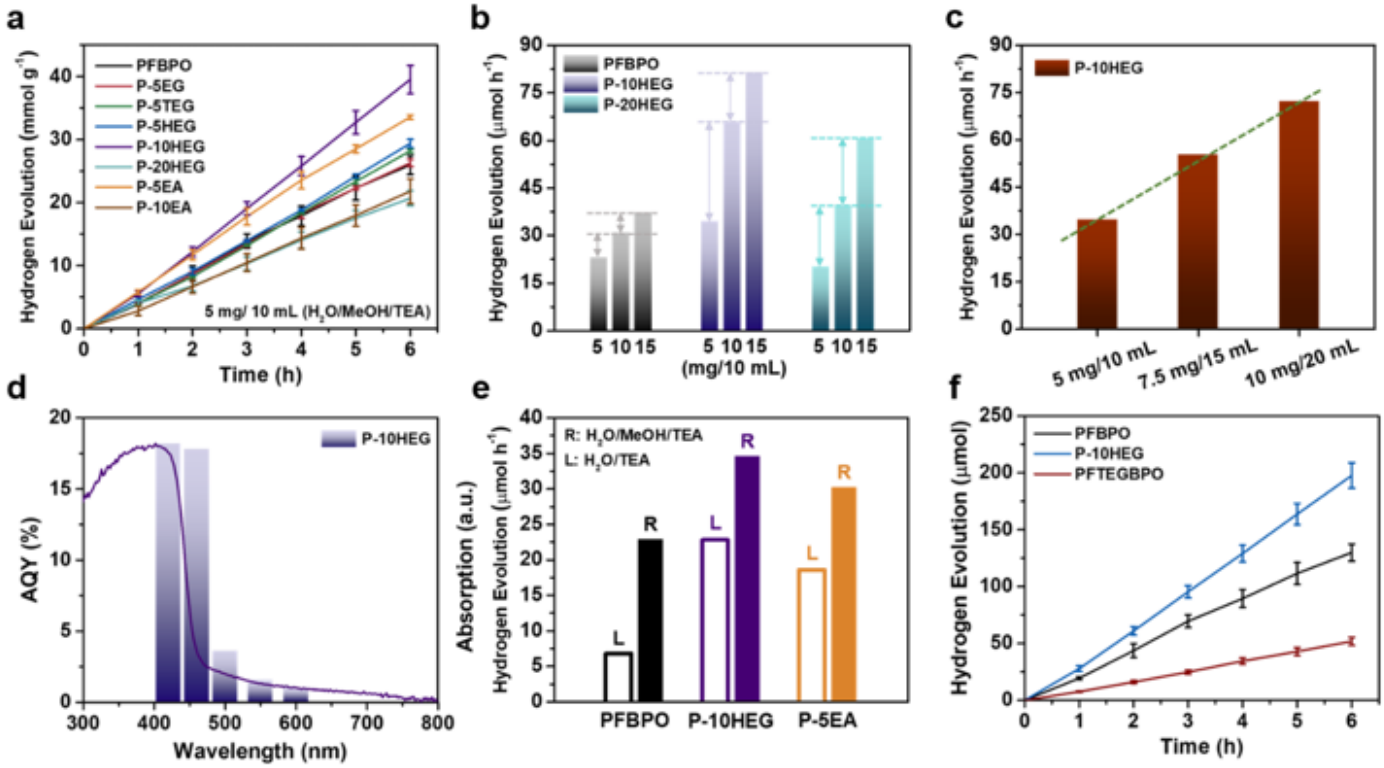

Figure 4

Photocatalytic hydrogen evolution experiments in solution. a Time-dependent HER of DCP and PFBPO photocatalysts under 380–780 nm irradiation. **b** Concentration dependence of the HER over PFBPO, P-10HEG, and P-20HEG. **c** Linear relationship between the HER and the quantity of photocatalytic solution (10, 15, and 20 mL of solution with a constant P-10HEG concentration. **d** Correlation between the apparent quantum yield (AQY) and the UV-vis absorption spectra of P-10HEG. **e** HER values in the absence of MeOH over PFBPO, P-10HEG, and P-5EA (L columns) compared to the HER values in presence of MeOH (R columns). **f** Comparison of the time-dependent HER over P-10HEG, PFBPO, and PFTEGBPO using the same photocatalytic conditions as used in Fig. 4a.

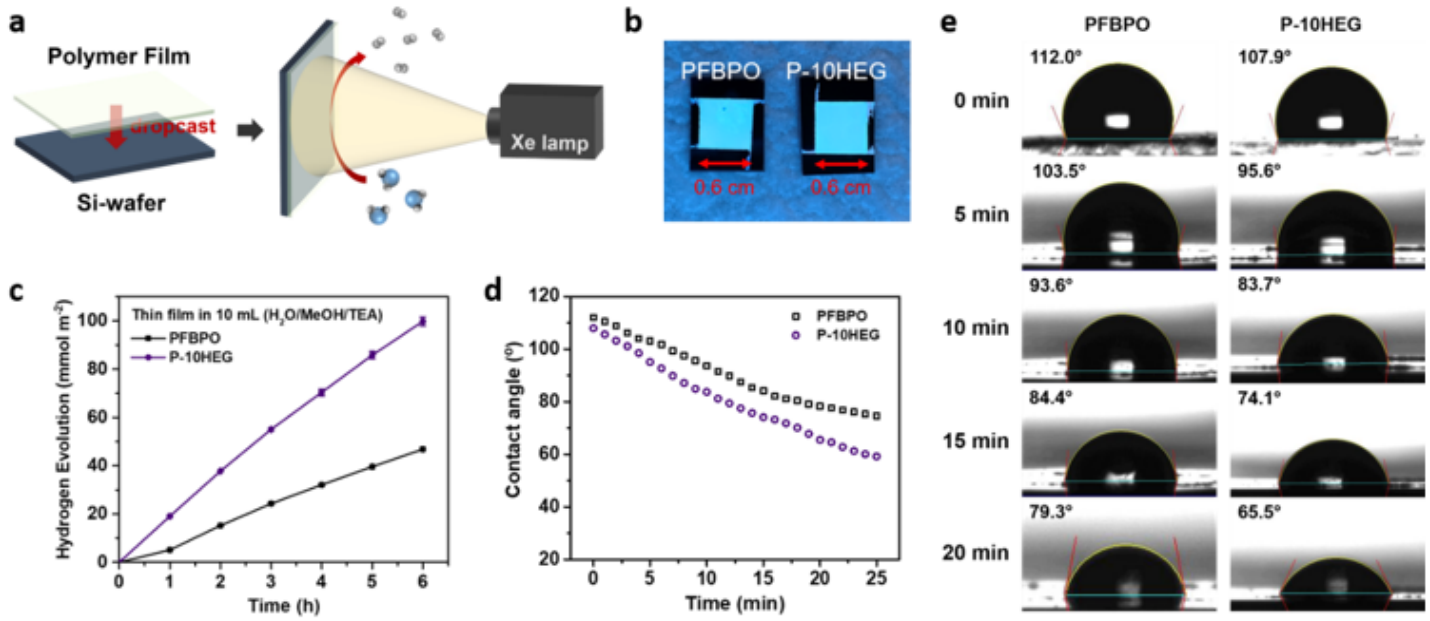

Figure 5

Photocatalytic hydrogen evolution experiments in film. a Schematic illustration of the photocatalytic hydrogen evolution in film systems. **b** Images of the 0.6 ´ 0.6 cm^2 film over PFBPO and P-10HEG. **c** Time-dependent HER of PFBPO and P-10HEG film immersed in 10 mL of a H_2O/MeOH/TEA solution under 380–780 nm irradiation. **d** Correlation between the time and the water contact angles of PFBPO and P-10HEG. **e** Time-dependence water contact angles of PFBPO and P-10HEG film.

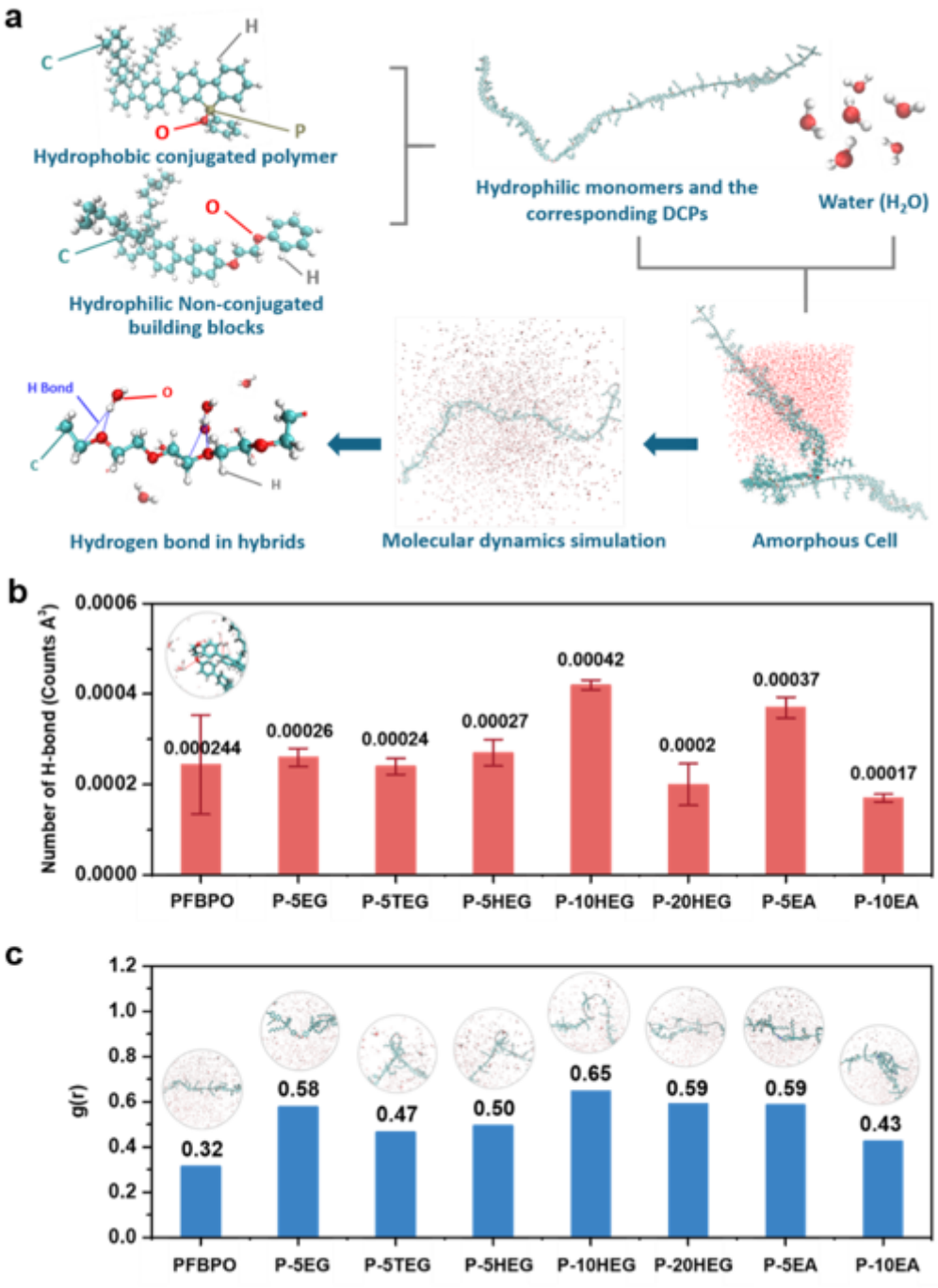

Figure 6

Molecular dynamics simulations. a The workflow of molecular dynamics study. The conjugate polymer models were built according to the overall mass and different repetition units. The system was filled with water in an amorphous cell to evaluate the hydro-bonding. **b** The statistics of hydrogen bounds and **c** the possibility of hydrogen bond formation of polymer photocatalysts.

Supplementary Files

This is a list of supplementary files associated with this preprint. Click to download.

- ESI.pdf